

$10^{-15} \text{ N}/\text{Å}^2$). Friction is an important concern in small-scale systems such as microelectromechanical systems (MEMS) (10), and recent atomic-scale frictional force measurements (11, 12) using conventional materials yield values about three orders of magnitude greater than the upper-limit frictional forces found here for MWNT surfaces.

If the (already generally small) friction between nanotube shells is indeed proportional to the length of the overlapping sections, then minimum bearing friction would be obtained for the shortest possible nanotube core-housing overlap. Several possibilities exist to achieve this configuration. First, a very short MWNT might be used from the outset. Second, the core of a long MWNT could be telescoped nearly all the way out, yielding a short contact area. The third possibility takes advantage of "bamboo" configurations (13) that sometimes occur in MWNTs, where the inner nanotube sections do not extend along the entire length of the MWNT, but rather represent an end-to-end series of shorter, fully capped, nanotube segments residing inside the continuous housing of outer nanotube shells. A TEM image of such a bamboo joint inside a larger MWNT is shown in Fig. 4A. In Fig. 4B, the core segment on the right has been telescoped out, cleanly separating the bamboo joint. This result shows that bamboo nanotube core segments are truly independent sections with weak end-to-end binding. This observation has important practical implications for common-axis bearings: Short independent bamboo sections might serve as ultralow-friction linear or rotational bearings that are firmly embedded in a common long, stiff cylindrical housing.

Our results demonstrate that MWNTs hold great promise for nanomechanical or nanoelectromechanical systems (NEMS) applications. Low-friction, low-wear nanobearings and nanosprings are essential ingredients in general NEMS technologies. The transit time for complete nanotube core retraction (on the order of 1 to 10 ns) implies the possibility of exceptionally fast electromechanical switches.

References and Notes

1. S. Iijima, *Nature* **354**, 56 (1991).
2. A. Kolmogorov and V. Crespi, *Bull. Am. Phys. Soc.* **45**, 254 (2000).
3. V. H. Crespi, P. Zhang, P. E. Lammert, in *Electronic Properties of Novel Materials—Science and Technology of Molecular Nanostructures*, H. Kuzmany, J. Fink, M. Mehring, S. Roth, Eds. (American Institute of Physics, College Park, MD, 1999), pp. 364–368.
4. H. D. Wagner, O. Lourie, Y. Feldman, R. Tenne, *Appl. Phys. Lett.* **72**, 188 (1998).
5. M. F. Yu et al., *Science* **287**, 637 (2000).
6. J. Cummings, P. G. Collins, A. Zettl, *Nature*, in press.
7. P. Poncharal, Z. L. Wang, D. Ugarte, W. A. De Heer, *Science* **283**, 1513 (1999).
8. L. X. Benedict et al., *Chem. Phys. Lett.* **286**, 490 (1998).
9. B. N. J. Persson, *Surf. Sci. Rep.* **33**, 83 (1999).
10. W. Trimmer, *Micromechanics and MEMS: Classic and Seminal Papers to 1990* (IEEE Press, New York, 1997).
11. R. W. Carpick, D. F. Ogletree, M. Salmeron, *Appl. Phys. Lett.* **70**, 1548 (1997).

12. M. Enachescu et al., *Phys. Rev. Lett.* **81**, 1877 (1998).
13. S. Iijima, P. M. Ajayan, T. Ichihashi, *Phys. Rev. Lett.* **69**, 3100 (1992).
14. We thank U. Dahmen, C. Nelson, E. Stach, M. L. Cohen, and S. G. Louie for helpful interactions. Supported by the Office of Energy Research, Office of

Basic Energy Sciences, Division of Materials Sciences, U.S. Department of Energy (contract DE-AC03-76SF00098) and by NSF grants DMR-9801738 and DMR-9501156.

9 March 2000; accepted 21 June 2000

Full Three-Dimensional Photonic Bandgap Crystals at Near-Infrared Wavelengths

Susumu Noda,^{1*} Katsuhiko Tomoda,¹ Noritsugu Yamamoto,² Alongkarn Chutinan¹

An artificial crystal structure has been fabricated exhibiting a full three-dimensional photonic bandgap effect at optical communication wavelengths. The photonic crystal was constructed by stacking 0.7-micrometer period semiconductor stripes with the accuracy of 30 nanometers by advanced wafer-fusion technique. A bandgap effect of more than 40 decibels (which corresponds to 99.99% reflection) was successfully achieved. The result encourages us to create an ultra-small optical integrated circuit including a three-dimensional photonic crystal waveguide with a sharp bend.

There is much interest in photonic crystals (1–3) in which the refractive index changes periodically. A photonic bandgap is formed in the crystals, and the propagation of electromagnetic waves is prohibited for all wave vectors. Various scientific and engineering applications, such as control of spontaneous emission, zero-threshold lasing, sharp bending of light (4), and so on, are expected by using the photonic bandgap and the artificially introduced defect states and/or light-emitters. To realize the potential of photonic crystals as much as possible, the following requirements should be satisfied: (i) construction of a three-dimensional (3D) photonic crystal with a complete photonic bandgap in the optical wavelength region, (ii) introduction of an arbitrary defect state into the crystal at an arbitrary position, (iii) introduction of an efficient light-emitting element, and (iv) use of an electronically conductive crystal, which is desirable for the actual device application. Although various important approaches such as a self-assembled colloidal crystal (5), a GaAs-based three-axis dry-etching crystal (6), and a silicon-based layer-by-layer crystal (7, 8) with a so-called woodpile structure (9) have been proposed and investigated to construct the 3D photonic crystals, it is considered difficult for these methods to satisfy the four above requirements simultaneously.

¹Department of Electronic Science and Engineering, Kyoto University, Yoshida-honmachi, Sakyo-ku, Kyoto 606-8501, Japan. ²Electrotechnical Laboratory, Agency of Industrial Science and Technology (AIST), Ministry of International Trade and Industry (MITI), 1-1-4, Umezono, Tsukuba, Ibaraki, 305-8568, Japan.

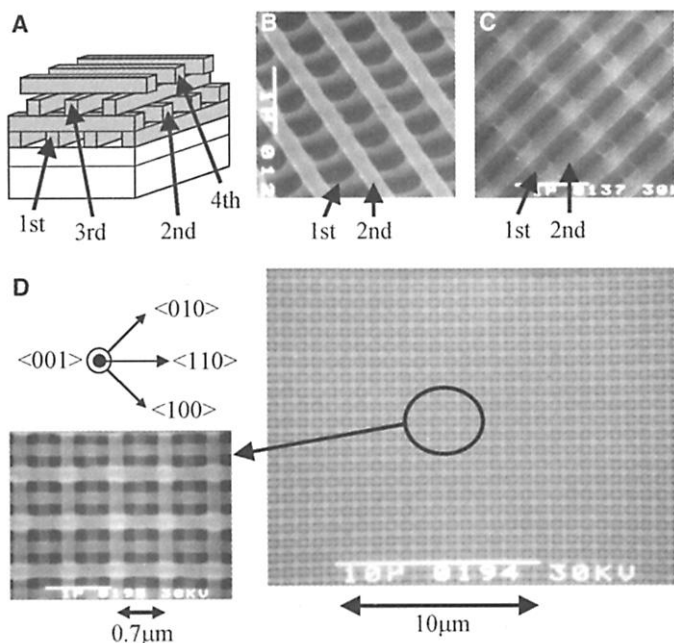
*To whom correspondence should be addressed. E-mail: snoda@kuee.kyoto-u.ac.jp

Recently, we reported a complete 3D photonic crystal at infrared (5 to 10 μm) (10–12) to near-infrared wavelengths (1 to 2 μm) (12) based on a method in which III-V semiconductor stripes are stacked with the wafer-fusion and laser beam-assisted very precise alignment techniques to construct the woodpile structure. Because the crystal is constructed with III-V semiconductors, which are widely used for optoelectronic devices, the above requirement (iii) is satisfied. Moreover, as the wafer-fusion technique enables us to construct an arbitrary structure and to form an electronically active interface, all requirements (i) through (iv) will be satisfied.

However, an important issue remains to be solved: the photonic crystal with sufficient bandgap effects has not yet been realized at near-infrared wavelengths. The bandgap effect at near-infrared wavelengths was much weaker (by more than a factor of 10) than those at infrared wavelengths. A very weak effect was observed also in silicon-based layer-by-layer crystals (8). This is certainly due to the structural fluctuations caused by the imperfection of material process when the size is in the sub-micrometer range, which leads to serious problems for the actual scientific applications such as complete control of spontaneous emission and very sharp bending of light. We developed the advanced processing technique to address the above issue and to fabricate 3D photonic crystals with sufficient bandgap effects at near-infrared wavelengths. It is also shown that the crystal is applicable to ultra-small optical integrated circuits, including a 3D waveguide with a sharp bend.

In the crystal structure studied here (Fig. 1A), where one unit of woodpile structure is

Fig. 1. (A) Schematic drawing of one unit of woodpile-structure 3D photonic crystal. (B and C) SEM images of the stacked two stripes fabricated in a previous report (12) and here, respectively. (D) SEM image of 3D photonic crystal fabricated with advanced processing techniques.



illustrated, the structure is expected to have a complete bandgap of $\sim 16\%$ at the normalized frequency region of $\sim 0.6 [c/a]$, where c is the light velocity and a is the lattice constant defined as $\sqrt{2}$ times stripe period. The crystal is constructed by stacking single crystalline III-V semiconductor (GaAs or InP) stripes as follows: A pair of striped wafers is first wafer-fused at 700°C with crossed configuration, and then one of the substrates is removed by a combination of chemical- and dry-etching processes. Then, a pair of wafers with two stacked striped layers is stacked again by wafer-fusion technique such that two parallel stripes (1st and 3rd and 2nd and 4th) are shifted by half a period to construct the structure (Fig. 1A) with a laser beam-assisted alignment method. Again, one of the substrates is removed. We have carefully examined these processes to find the main factors of structural fluctuations, for example, the discrepancy between the formed stripe patterns and the designed ones, the alignment accuracy between the parallel stripes, and so on. We found that the most important factor is the degradation of stripe patterns caused by (i) mass transport during the wafer-fusion process at 700°C and (ii) over-etching after the substrate-removing process. A scanning electron microscope (SEM) image (Fig. 1B), taken after the wafer-fusion and substrate-removing processes, shows that the stripe edge is rounded and the thickness of the stripes becomes very thin, especially at the center. The degradation was found to be serious when the stripe period was in the submicrometer range ($0.7 \mu\text{m}$), as it was here. The effects of the fluctuations have been theoretically investigated with super cell-based plane wave-expansion method (13) and/or transfer-matrix method (14) by introducing these fluctuations; we found that the bandgap effect is reduced by more than a factor of 10. To

solve the problems, we investigated the most appropriate wafer-fusion temperature at which mass-transport phenomenon is suppressed sufficiently but the bonding is strong enough, by changing the temperature from 700° to 400°C . We found that 500°C is most appropriate. To avoid the over-etching phenomenon, we used an interference method to control the etching depth strictly, where the interference color from the stacked stripes is monitored during the etching process. The

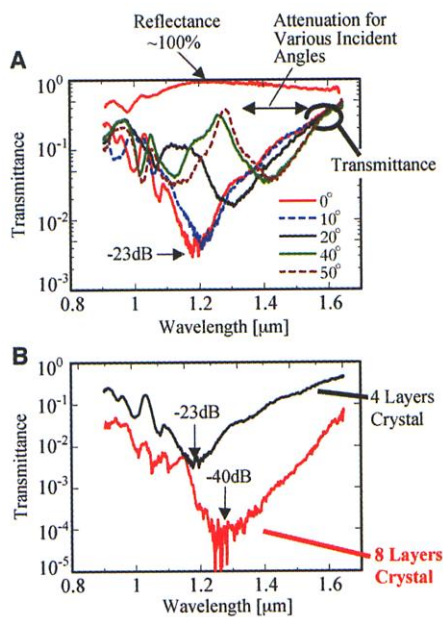


Fig. 2. (A) Normal incident transmission and reflection spectra, together with the transmission spectra for various incident angles from 0° to 50° for the Fig. 1D crystal. (B) Transmission spectra for the eight-layer crystal, where the spectra of the four-layer crystal is also shown for comparison.

degradation of stripe patterns was suppressed sufficiently with these advanced processing techniques (Fig. 1C). Figure 1D shows the SEM of the one unit of photonic crystal developed here. The structure is constructed in a wide area, and the expanded view shows that the crystal is perfectly constructed within the accuracy of 30 nm , even in the case of a small stripe period of $0.7 \mu\text{m}$.

Normal incident transmission and reflection spectra of the Fig. 1D crystal are shown in Fig. 2A, together with the transmission spectra for various incident angles. The maximum attenuation as large as 23 dB was successfully observed at the $1\text{-}2\text{-}\mu\text{m}$ wavelength region, and, correspondingly, maximum reflectance of almost 100% has been observed. The result indicates that the bandgap effect increases by a factor of more than 10 compared with the results achieved previously (8 to 10 dB) (8, 12), which means that the crystal is indeed perfect structure from the viewpoint of the optical properties. In Fig. 2A, the transmission spectra for various incident angles are also indicated. The angles were changed from 0° to 50° from $\langle 001 \rangle (\Gamma\text{-X}')$ to $\langle 110 \rangle (\Gamma\text{-K}'')$ directions. As can be seen in Fig. 2A, the wavelength at which the transmittance becomes minimum shifts to the longer wavelength with increasing incident angles, and the shift tends to saturate at 40° to 50° . The result coincides with the theoretical result. When the full-bandgap wavelength region is defined as the range at which the attenuation becomes more than 80% , it covers ~ 1.3 to $1.55 \mu\text{m}$, which is very important for the optical communication field.

To extend the above results, we created the crystal with two-unit structure (eight stacked stripes). The normal incident transmission spectrum is shown in Fig. 2B, together with that of a one-unit crystal. The attenuation of more than 40 dB (which corresponds to 99.99% reflection) was observed. The bandgap effect at the wavelengths corresponding to the full bandgap (1.3 to $1.55 \mu\text{m}$) was much more enhanced.

These results encourage us to develop

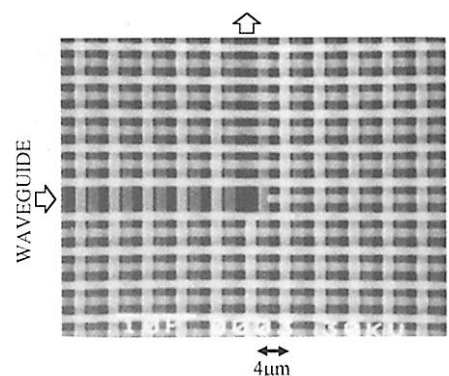


Fig. 3. SEM image of 3D sharp bend (90°) waveguide developed here.

ultra-small optical circuits based on the 3D photonic crystal. Figure 3 shows the first successful fabrication of 3D sharp bend (90°) waveguide, which has been developed here. Two stripe layers, one of which is removed to form a straight air waveguide, are stacked with a crossed configuration to form a 90° bend waveguide, and they are sandwiched by the upper and lower complete photonic crystals. The waveguide is composed of 12 stacked layers in total with a stripe period of 4 μm. The waveguide has a potentially very high transmission (>95%) property in a very

wide frequency range from 0.553 to 0.605 [c/a], which was predicted by the finite-difference time-domain calculation (15).

References

1. E. Yablonovitch, *J. Opt. Soc. Am. B* **10**, 283 (1993).
2. S. John, *Phys. Today* **44**, 32 (1991).
3. J. D. Joannopoulos, P. R. Villeneuve, S. Fan, *Nature* **386**, 143 (1997).
4. A. Mekis et al., *Phys. Rev. Lett.* **77**, 3787 (1996).
5. V. N. Astratov et al., *Nuovo Cimento D* **17D**, 1349 (1995).
6. V. Arbel-Engels et al., in *Microcavities and Photonic Bandgaps*, J. Rarity and C. Weisbuch, Eds. (Kluwer Academic, Boston, 1996), pp. 125–131.
7. S. Y. Lin et al., *Nature* **394**, 251 (1998).

8. J. G. Fleming and S. Y. Lin, *Opt. Lett.* **24**, 49 (1999).
9. K. M. Ho, C. T. Chan, C. M. Soukoulis, R. Biswas, M. Sigalas, *Solid State Commun.* **89**, 413 (1994).
10. N. Yamamoto and S. Noda, Proceedings of the Tenth International Conference on Indium Phosphide and Related Materials FB2-2, Tsukuba, Japan, 11 to 15 May 1998 (IEEE Catalog #98H36129, Piscataway, NJ, 1998).
11. N. Yamamoto, S. Noda, A. Chutinan, *Jpn. J. Appl. Phys.* **37**, L1052-4 (1998).
12. S. Noda, N. Yamamoto, H. Kobayashi, M. Okano, K. Tomoda, *Appl. Phys. Lett.* **75**, 905 (1999).
13. A. Chutinan and S. Noda, *J. Opt. Soc. Am. B* **16**, 240 (1999).
14. _____, *J. Opt. Soc. Am. B* **16**, 1398 (1999).
15. _____, *Appl. Phys. Lett.*, **75**, 3739 (1999).

20 March 2000; accepted 5 June 2000

Synthesis and Characterization of Helical Multi-Shell Gold Nanowires

Yukihito Kondo^{1*†} and Kunio Takayanagi^{1,2}

Suspended gold nanowires were made in an ultra-high vacuum. The finest of them was 0.6 nanometer in diameter and 6 nanometers in length. By high-resolution electron microscopy, they were shown to have a multi-shell structure composed of coaxial tubes. Each tube consists of helical atom rows coiled round the wire axis. The difference between the numbers of atom rows in outer and inner shells is seven, resulting in magic shell-closing numbers.

Metal nanowires suspended between two electrodes have attracted much interest in recent years because the electron transport properties of a quantum wire are of importance in fundamental physics and in electronic device technology. The metal nanowires have been made with a scanning tunneling microscope (STM) and by other methods (1–5). The conductances in these experiments were quantized in units of $2e^2/h$, where e is the electron charge and h is Planck's constant (6, 7). A recent experiment by simultaneous STM-TEM (transmission electron microscopy) clarified the structure and the conductance of gold nanowires (5). The contact in the experiment was not always a narrow neck; a wire (diameter <2 nm) was formed when the two electrodes faced each other in the [110] direction. However, the length of the wire was only 1 to 2 nm, too short for a conducting wire.

Long metal nanowires were predicted in a recent theoretical paper (8) to have “weird” structures that differ from the crystalline bulk. A helical structure was predicted for lead and aluminum nanowires. Carbon nano-

tubes also have helical structure (9) and are metallic or semiconducting, depending on the tube's chirality (10–13). Interesting physics may arise for long metal nanowires free from any supporting substrate.

Here, we report experimental evidence for multi-shell helical gold nanowires. High-resolution electron microscope images show that gold nanowires (<1.5 nm in diameter) consist of coaxial tubes. Each tube consists of helical atom rows coiled round the wire axis. The difference between the number of helical atom rows in outer and inner shells is seven, resulting in magic shell-closing numbers.

Gold nanowires were formed in an UHV (ultra-high vacuum)-TEM with the electron beam thinning technique reported previously (14). A gold (001) film 3 to 5 nm in thickness was cleaned by electron beam irradiation for 3 to 5 hours until the film showed the 5×20 reconstructed surface (15–17) at the specimen stage of the TEM, whose vacuum was 3×10^{-8} Pa. The film was subsequently irradiated with a very intense electron beam (200 kV, 500 A/cm²) until some holes were formed (14, 17, 18). When the bridge between two neighboring holes was narrowed, it became a long nanowire (5 to 15 nm) along the [110] direction. These nanowires (>1.5 nm in diameter) had a face-centered-cubic (fcc) structure in the core, and the lateral surfaces were reconstructed, forming a {111}-like close-packed structure (14). Thinned further by a weaker electron beam (10

to 50 A/cm²), they exhibited new structures with widths (diameters) of 0.6 to 1.5 nm and lengths of 3 to 15 nm. The above procedure was successful only under UHV and with well-cleaned samples. We analyzed videotapes recording the thinning process of over 30 wires (a total of 10 hours of recording).

The electron microscope images in Fig. 1, A through D, show four structures that were observed during the thinning. The diameters of these wires were 1.3, 1.2, 0.9, and 0.6 nm. The dark dots in the images represent the gold atoms (or gold lattice). These dots are not arranged regularly as in the fcc lattice. The lattice fringes obliquely intersect the wire axis at an angle of 60°, whereas in a fcc lattice they would intersect at 90°. The wire images appear wavy and are asymmetrical with respect to the wire axis. Closer inspection of the images revealed that the dark dots are aligned on a line along the wire axis, which represents an atom row. In contrast to crystalline lattices, these atom rows are not straight but have wavy modulation (particularly in Fig. 1D).

During the thinning process, the wire images changed drastically when the width changed. Occasionally, the image changed even when the width remained unchanged. The duration of the steady state of the wire became shorter as the wire became thinner. We carefully selected images that showed only the steady state of the wires from the large number of frame images captured from the videotape (time interval of digitization is 1/30 s). One of the finest wires stayed for ≈0.5 s before it ruptured. We measured the distance (d) between the dark dots on each atom row and the width (D) of the wire on the selected images. As shown in Fig. 2 (upper part), d was almost the nearest neighbor distance of gold (0.288 nm) for all the wires with $0.5 \text{ nm} < D < 1.5 \text{ nm}$. Although the histogram did not take the residence time (duration of the steady state) into account, the histogram for D (lower part of Fig. 2) shows peaks at $D = 0.58, 0.88, (0.96), 1.03, 1.13, 1.20, 1.29, \text{ and } 1.4 \text{ nm}$, reflecting the stable diameters of the gold wires. We constructed structure models that explained the magic peaks in Fig. 2 and carried out TEM

¹Takayanagi Particle Surface Project, Exploratory Research for Advanced Technology (ERATO), Akishima, Tokyo, 196-8558, Japan. ²Tokyo Institute of Technology, Nagatuta, Midori-ku, Yokohama, Japan.

*Present address: Japan Electron Optics Laboratory (JEOL) Ltd., Akishima, Tokyo, 196-8558, Japan.

†To whom correspondence should be addressed. E-mail: kondo@jeol.co.jp